Giant nonvolatile resistive switching in a Mott oxide and ferroelectric hybrid (SI Appendix)

Pavel Salev, Javier del Valle, Yoav Kalcheim, Ivan K. Schuller

Department of Physics and Center for Advanced Nanoscience, University of California San Diego, La Jolla, CA 92093, USA

X-ray diffraction of V_2O_3/PMN-PT

Fig. S1*A* shows a series of x-ray θ-2θ scans recorded in a V_2O_3/PMN-PT sample at different tilt (χ angle) and polar (φ angle) orientations. The V_2O_3 film grows having the (001) plane, i.e. the corundum *c*-plane, parallel to the PMN-PT (111) plane. The [100] direction in the V_2O_3 lattice is aligned with the [0 $\bar{1}$ 1] direction in the PMN-PT. Due to the lattice mismatch, the PMN-PT (111) plane was expected to induce a compressive strain in the *c*-plane of V_2O_3 film. However, the obtained lattice parameters of V_2O_3 film are a = 5.01 Å and c = 13.85 Å, which correspond to the tensile in-plane strain of +1.0% and compressive out-of-plane strain of -1.1% compared to the bulk crystal (1, 2). It is likely that the lattice-mismatch strain in V_2O_3 film relaxed during the high-temperature growth, and the observed strain built up during the after-growth cooling from 650 °C to room temperature. Because the thermal expansion coefficients of V_2O_3 (3) are larger compared to the PMN-PT (4), the substrate can induce a tensile in-plane strain in the film, which is consistent with the x-ray measurements. Fig. S1*B* shows the x-ray reflectivity of V_2O_3/PMN-PT. The data were corrected for the geometrical factors and were fitted using Motofit software. The obtained film thickness and roughness are 80 nm and 0.8 nm, respectively. Note that the roughness of the film corresponds to approximately half of the V_2O_3 unit cell size along the corundum *c*-axis

www.pnas.org/cgi/doi/10.1073/pnas.1822138116

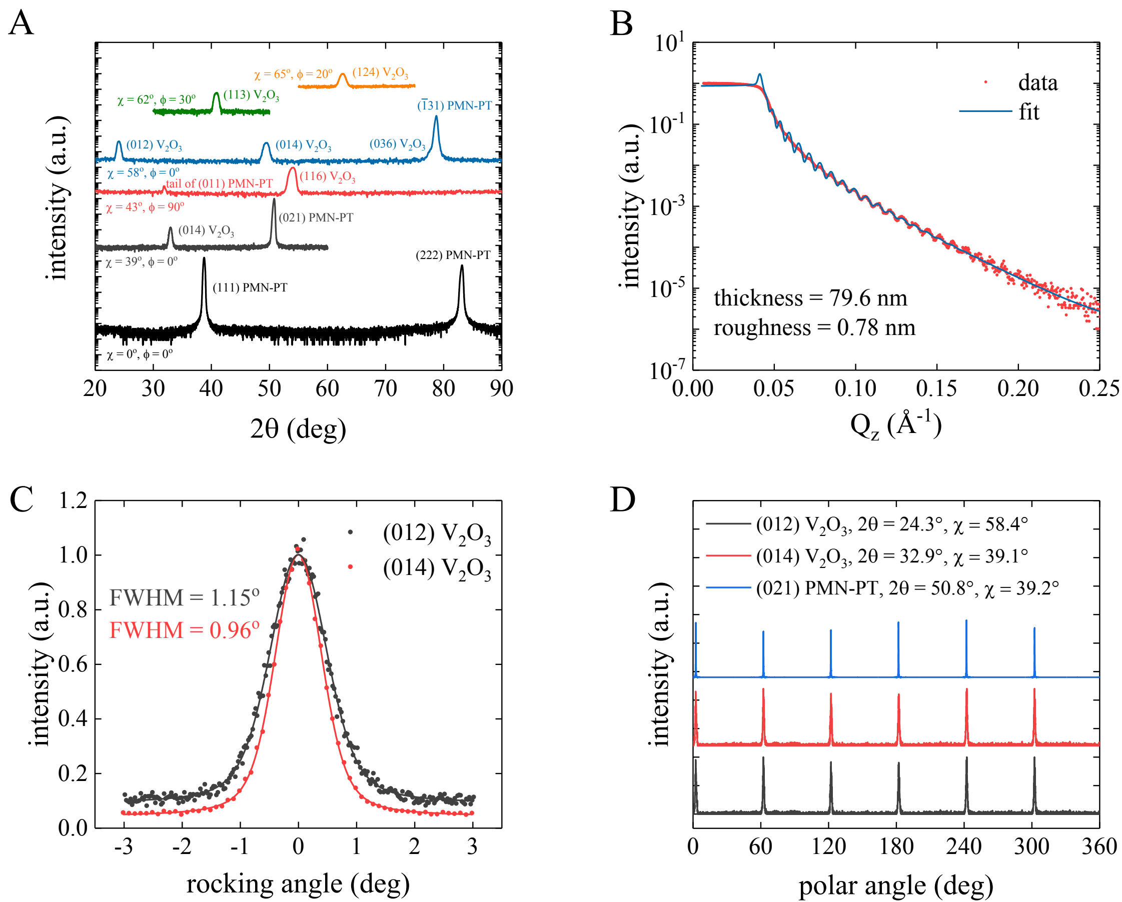

Fig. S1. X-ray diffraction of V_2O_3/PMN-PT. *(A)* A series of θ-2θ scans recorded at different tilt (χ angle) and polar (φ angle) orientations. *(B)* X-ray reflectivity. A correction for the x-ray beam footprint has been applied to the experimental data before the fitting. *(C)* Rocking scans. *(D)* Pole figures.

direction. This indicates a very smooth growth of the V_2O_3 layer. Fig. S1*C* shows the rocking curves of (012) and (014) Bragg peaks of V_2O_3. The full width at half maximum is approximately 1°, which suggests a highly textured growth of the film. Fig. S1*D* shows the pole figures of (012) V_2O_3, (014) V_2O_3, and (021) PMN-PT peaks. The peaks have 60° periodicity and are perfectly aligned with respect to each other. This indicates that the PMN-PT substrate does determine the orientation of the growing V_2O_3 film.

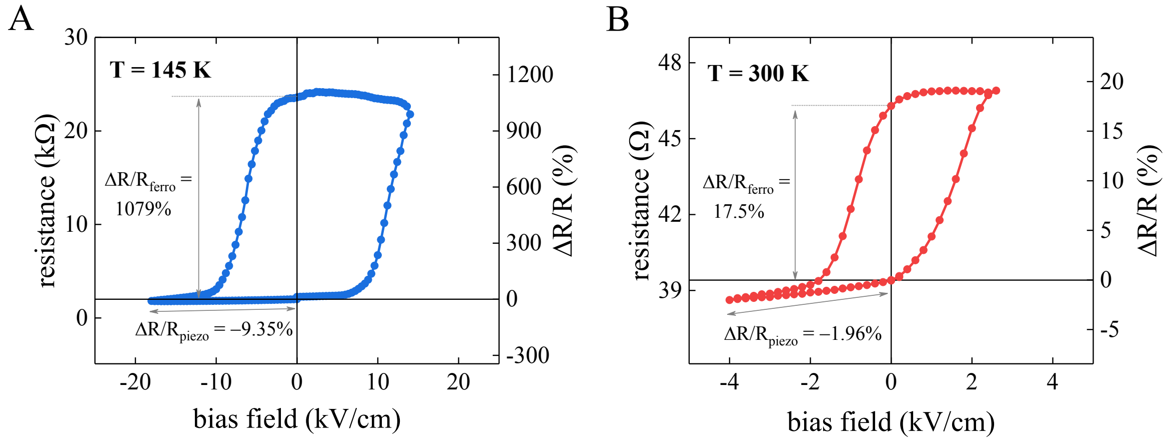

Fig. S2. Piezoelectric vs. ferroelastic effects. *(A, B)* Resistance vs. bias field loops recorded at 145 K *(A)* and 300 K *(B)*. The volatile resistive modulation $\Delta R/R_{piezo}$ associated with the piezoelectric effect and the nonvolatile resistive switching $\Delta R/R_{ferro}$ associated with the ferroelastic switching are highlighted in the plots.

Resistive switching: ferroelastic vs. piezoelectric effects

In addition to the nonvolatile resistive switching in V_2O_3/PMN-PT, a small resistance modulation by an applied bias can be observed when the device is switched into the low-resistance state (Fig. S2). This modulation can be associated with the converse piezoelectric effect in PMN-PT, i.e. the strain is proportional to the applied bias field. The piezoelectric resistive modulation is volatile and it is much smaller, $\Delta R/R_{piezo} < 10\%$, compared to the nonvolatile resistive switching due to the ferroelastic switching, $\Delta R/R_{ferro}$ up to 1100%. The observation of the piezoectric-like resitance modulation in V_2O_3/PMN-PT provides further evidence that the transfer of strain from the PMN-PT into the V_2O_3 is at the origin of the giant resistive switching.

Comparison between the magnitudes of piezoelectric and ferroelastic strains

Fig. S3*A* shows three x-ray θ-2θ scans in the vicinity of (111) PMN-PT peak. The blue and the red lines were recorded at zero bias when the V_2O_3/PMN-PT sample was switched into the

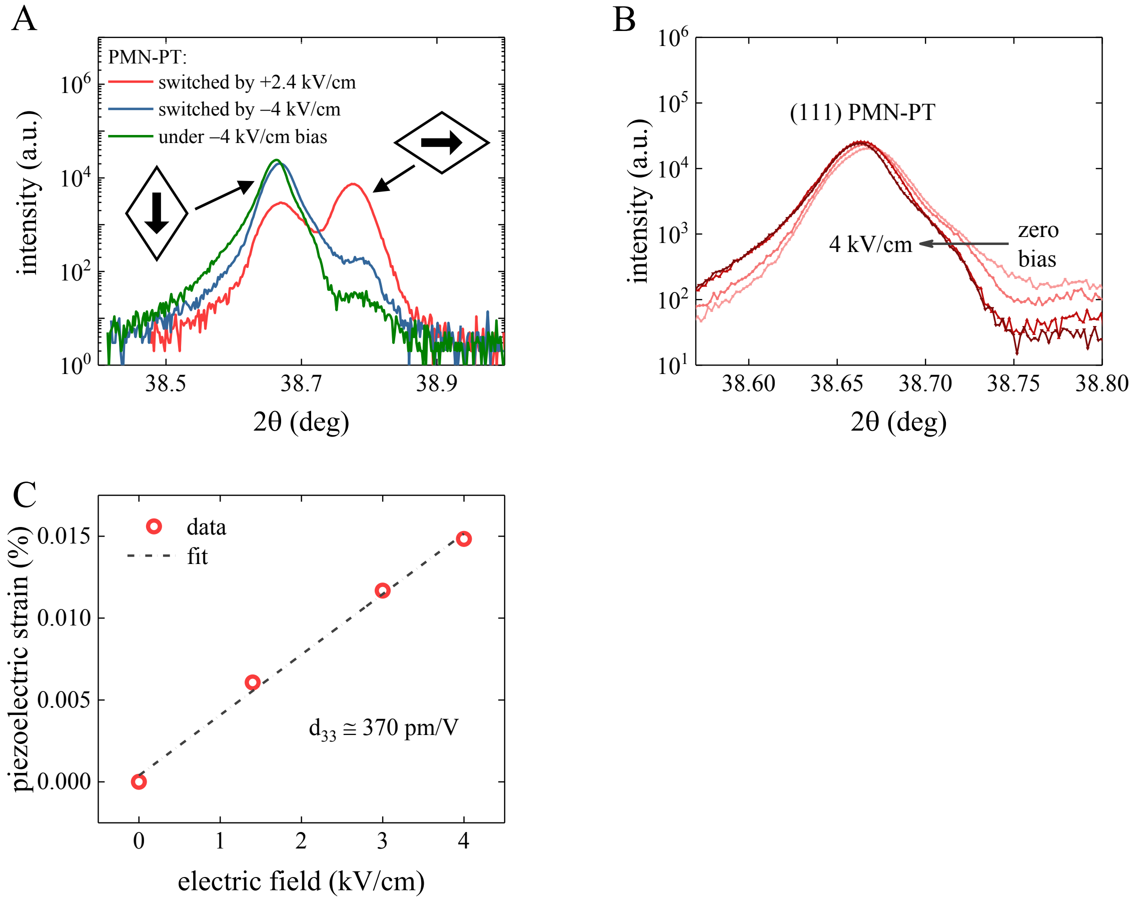

Fig. S3. Piezoelectric and ferroelastic strains in V_2O_3/PMN-PT. *(A)* θ-2θ scans near the (111) PMN-PT peak for the sample switched into the low- (blue line), high-resistance (red line) states, and under the *in-situ* application of -4 kV/cm bias (green line). *(B)* θ-2θ scans near the (111) PMN-PT peak under the *in-situ* application of 0…-4 kV/cm bias. *(C)* piezoelectric strain along the [111] direction in the PMN-PT as a function of the applied bias. The linear fit was used to extract the piezoelectric coefficient d_{33}.

low- and high-resistance states, respectively. The peak at 2θ = 38.67° corresponds to the scattering from the domains with the out-of-plane (OOP) polarization orientation, and the peak at 2θ = 38.78° is produced by the scattering from the domains with an in-plane (IP) polarization component. The ferroelastic strain associated with the polarization switching between the OOP and IP states is $\sigma_{ferro} = 100\%(d_{oop} - d_{ip})/d_{ip} = 0.27\%$, where d_{oop} (d_{ip}) is the spacing between PMN-PT (111) planes in the OOP (IP) domains. When the V_2O_3/PMN-PT is switched into the high-resistance state, the

fraction of the IP domains is approximately 40% as it can be estimated from the intensity distribution between the Bragg peaks corresponding to the OOP and IP domains (see Fig. 3*D* in the main text). The IP domains are at 71°/109° with respect to the surface normal because the polarization in PMN-PT is aligned with the space diagonals of the perovskite unit cell (5). Assuming that the sizes of polarization domains are much smaller compared to the V_2O_3/PMN-PT device, the average strain on the device's length-scale associated with the polarization multidomain state $\sigma_{domain} = 40\% \cdot \sin(71°) \cdot 0.27\% = 1.02 \cdot 10^{-2}\%$.

For comparison between the ferroelastic and piezoelectric strains, the diffraction pattern recorded under the application of -4 kV/cm bias *in-situ* to the V_2O_3/PMN-PT is shown on Fig. S3*A* (green line). The strain associated with the piezoelectricity is much smaller than the ferroelastic strain as can be inferred from a very small shift of the (111) peak. To obtain a numerical estimate of the piezoelectric strain in V_2O_3/PMN-PT, we measured the x-ray diffraction in the vicinity of (111) PMN-PT peak while applying *in-situ* 0…-4 kV/cm bias via electrical leads attached to the V_2O_3 film and Au electrode (Fig. S3*B*). By fitting the experimental data with the Voigt function, we calculated the piezoelectric strain as the function of bias field as $\sigma_{piezo}(E) = 100*(d_{111}(E) - d_{111}(0))/d_{111}(0)$ (Fig. S3*C*). Using the linear relation between the piezoelectric strain and the bias field $\sigma_{piezo} = d_{33} \cdot E$, we obtained the piezoelectric coefficient of the PMN-PT substrate along the <111> direction d_{33} = 370 pm/V. At room temperature the coercive field of the substrate is 2.4 kV/cm, i.e. the field at which the switching between the low- and high-resistance states takes place. The piezoelectric strain at the opposite field is $\sigma_{piezo}(-2.4 \text{ kV/cm}) = 8.9 \cdot 10^{-3}\%$. Now we can obtain an estimate of the ratio between σ_{domain} and σ_{piezo} strains. The lower bound of the strain ratio is $\sigma_{domain}(E_{c+})/\sigma_{piezo}(-E_{c+}) \sim 10$. Taking into account the PMN-PT's Poisson ratio, the upper bound of the strain ratio is $\sigma_{domain}(E_{c+})/\sigma_{piezo}(-E_{c+}) \sim 30$. The much smaller magnitude of the piezoelectric

strain can qualitatively explain why the piezoelectric-like resistance modulation $\Delta R/R_{piezo}$ in the V_2O_3 film is much smaller compared to the nonvolatile resistive switching $\Delta R/R_{ferro}$ due to the nucleation of IP polarization domains in the PMN-PT (Fig. S2).

Hydrostatic-pressure like model of the resistive switching in V_2O_3/PMN-PT

We considered a simple hydrostatic-pressure-like model (6) of the resistance vs. stress dependence in the V_2O_3/PMN-PT:

$$R = R_0 \exp\left(\frac{a\sigma}{k_B T}\right),$$

where σ is the stress exerted on the V_2O_3 by the PMN-PT, α is a phenomenological parameter, and k_B is the Boltzmann constant. This model is expected to apply only to the metallic state of V_2O_3 because a simple exponential law cannot account for the complexity of the MIT. To test the model, we examined the temperature dependence of the V_2O_3/PMN-PT resistance at the bias fields corresponding to the substrate's coercive field E_{c+} and the exact opposite field $-E_{c+}$ as defined in Fig. 4a. At the E_{c+} bias, the IP domains nucleate in the PMN-PT exerting a tensile stress $\sigma_{domain}(E_{c+})$ on the V_2O_3. The $-E_{c+}$ bias induces a piezoelectric contraction of the substrate's in-plane lattice parameters exerting a compressive stress $\sigma_{piezo}(-E_{c+})$ on the film. It should be noted that there is an important distinction between the stresses at $-E_{c+}$ and E_{c+}. The piezoelectric stress $\sigma_{piezo}(-E_{c+})$ is expected to be homogeneous on the length-scale of a V_2O_3/PMN-PT device, while the stress provided by switching the substrate into a multidomain state $\sigma_{domain}(E_{c+})$ is inherently non-uniform. The domain sizes in bulk ferroelectrics typically range on the 1 – 100 μm scale (7), which is much smaller compared to the size of a V_2O_3/PMN-PT device. Therefore, we consider an average $\sigma_{domain}(E_{c+})$ with respect to the volume ratio between IP and OOP domains in the PMN-PT. From the x-ray measurements, we estimated the stress ratio $\sigma_{domain}(E_{c+})/\sigma_{piezo}(-E_{c+}) \sim 10 - 30$ (see the

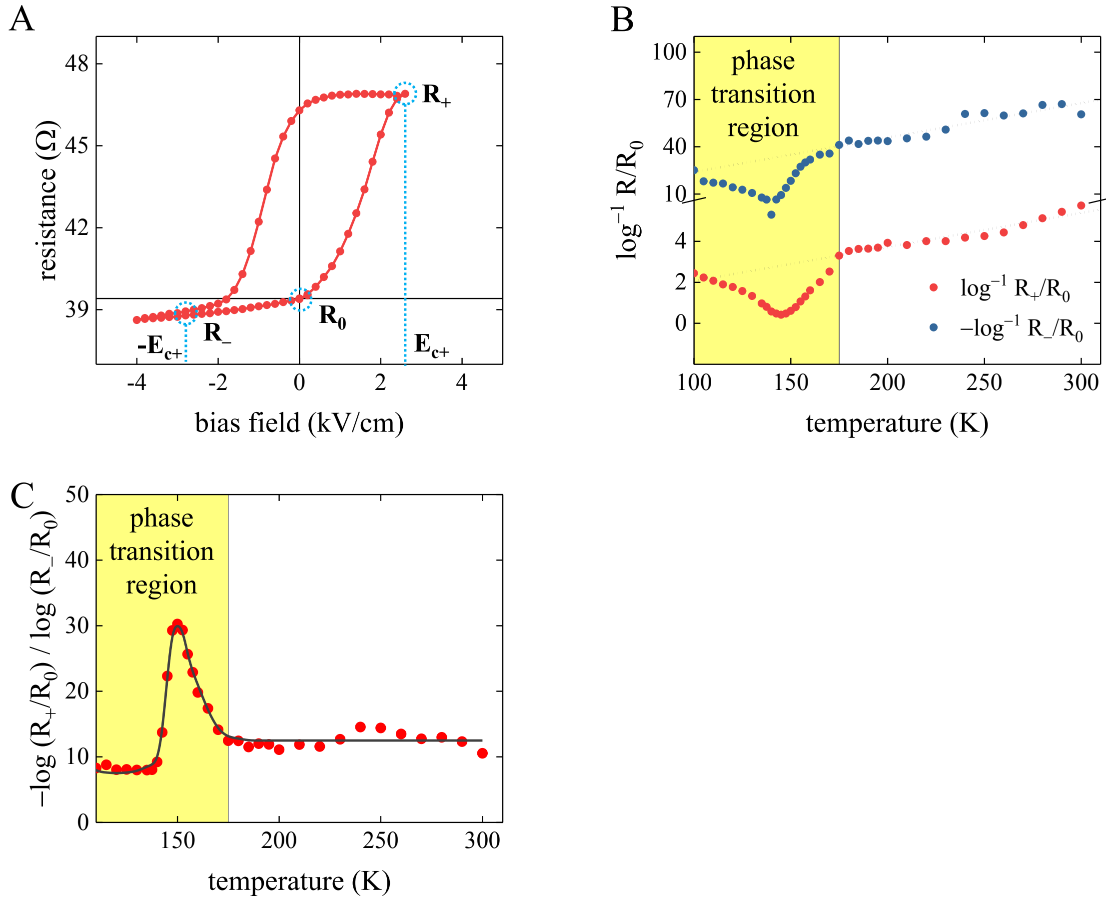

Fig. S4. Resistive switching model. *(A)* Resistive switching loop of V_2O_3/PMN-PT recorded at 300 K. Resistance values corresponding to a multidomain state in the PMN-PT at the coercive field $R_+(E_{c+})$, piezoelectric compression of the PMN-PT at the opposite field $R_-(-E_{c+})$, and the low-resistance state at zero bias R_0 are defined on the plot. *(B, C)* Comparison between the experimental data and the predictions of a simple exponential model of resistance vs. stress dependence. The reciprocal logarithm of resistance ratio *(B)* is expected to grow linearly with the temperature and the log-resistance ratio *(C)* is expected to be proportional to the strain ratio developing in a device at E_{c+} and $-E_{c+}$ bias fields. The lines are guides for the eye. The model is not expected to adequately describe the phase transition region (shaded in yellow).

previous section). Fig. S4*B* shows the temperature dependence of the $log^{-1} R/R_0$ for the resistance values recorded at E_{c+} (red dots) and $-E_{c+}$ (blue dots). According to the exponential model, this dependence should be linear. Indeed, above the MIT both $log^{-1} R_+/R_0$ and $log^{-1} R_-/R_0$ show a steady linear growth with the temperature. Fig. S4*C* shows the temperature

dependence of the log-resistance ratio $log\left({}^{R_+}/_{R_0}\right)/log\left({}^{R_-}/_{R_0}\right)$, which, according to the exponential model, should be equal to $\sigma_{domain}(E_{c+})/\sigma_{piezo}(-E_{c+})$. Above the MIT the log-resistance ratio remains close to 13. This is consistent with the estimate of the stress ratio obtained from the x-ray measurements. Deviations from the model are observed only in the vicinity of MIT, which is expected because this simple exponential model cannot describe the MIT. The hydrostatic-pressure-like model provides a surprisingly good description of the resistance modulation in V_2O_3/PMN-PT when the film is in the metallic state. Therefore, it is likely that the giant resistive switching in the vicinity of MIT is also driven by the transfer of switchable strain from the PMN-PT into the V_2O_3.

Contribution of disorder, ion migration, field-effect to the resistive switching in V_2O_3/PMN-PT

(i) Strain-mediated disorder

The resistive switching in the V_2O_3/PMN-PT coincides with switching the ferroelectric substrate into a polarization multidomain configuration. The strain that develops in a multidomain PMN-PT is inherently inhomogeneous. Therefore, this inhomogeneous strain can induce a structural disorder in the V_2O_3 film. A structural disorder due to radiation damage was previously reported to strongly influence the MIT in V_2O_3 films (8). Irradiation experiments found that the resistivity of metallic state of V_2O_3 increases upon introducing a disorder. This qualitatively agrees with the resistive switching in V_2O_3/PMN-PT: the film's resistance is always higher when the substrate is switched into a multidomain state. However, the structural disorder was reported to reduce the T_c of V_2O_3, which is in the stark contrast with the observations in V_2O_3/PMN-PT. We found that the T_c of V_2O_3 film increases by up to 32 K when the PMN-PT is in the disordered

multidomain state (see Fig. 1 *C-D* in the main text). Therefore, the direct strain effect, i.e. stretching/compressing of the V_2O_3 lattice by the IP/OOP polarization domains in the PMN-PT, rather than a strain-mediated disorder associated with the mixed IP-OOP state, is most likely responsible for the resistive switching and T_c modulation in the V_2O_3/PMN-PT.

(ii) Ion migration

During the polarization switching in the PMN-PT, large transient currents can flow through the V_2O_3 layer to compensate for the sudden change of the bound charge at the V_2O_3/PMN-PT interface. For example, because the spontaneous polarization of PMN-PT is approximately 0.4 C/m^2 (see Fig. 1*B* in the main text), an electric current density of 4 – 400 A/m^2 can flow through the V_2O_3 layer if the polarization switching occurs on 1 – 100 ms timescale. The electroforming in V_2O_3 films has been previously reported in the literature: some parts of a V_2O_3 film can transform into other VO_x phases under the application of a strong electric stimulus (9). In V_2O_3/PMN-PT, however, the observed resistance vs. bias field loops are not consistent neither with bipolar nor unipolar electroforming-induced resistive switching (see Fig. 3 *A-C* in the main text). In the bipolar electroforming-induced resistive switching, the initial resistance state of a device could be recovered only by the application of an opposite polarity bias. In V_2O_3/PMN-PT, a large magnitude bias that saturates the PMN-PT's polarization in the out-of-plane direction always switches the V_2O_3 in the low-resistance state (see Fig. 3*A* in the main text). The high-resistance state emerges at intermediate bias fields close to the positive and negative coercive fields of the PMN-PT, but further incense of the applied bias, unlike in the bipolar electroforming-induced switching, leads to the recovery of the low-resistance state. In the unipolar electroforming-induced resistive switching, the low-resistance state can be recovered only by applying a high voltage to a device. On the contrary, the low-resistance state of V_2O_3/PMN-PT can be recovered

by an opposite polarity bias with a magnitude smaller than it is required to induce the high-resistance state (see Fig. S2, S4A and Fig. 2*A*, 3 *B-C* in the main text). Furthermore, the R-T measurements (see Fig. 1*C* in the main text) did not reveal the presence of other VO_x phases which could be identified by the MIT transitions at temperatures different from the T_c of V_2O_3 (9). Therefore, it is unlikely that the transient currents associated with the polarization switching in the PMN-PT could cause such an ion migration that can strongly change the resistance of V_2O_3 film.

(iii) Field-effect

The "butterfly" shape of the ΔR/R vs. E loop (see Fig. 3*A* in the main text) rules out the possibility that the resistive switching in the V_2O_3/PMN-PT is due to the field-effect. The electrostatic screening of the spontaneous polarization of PMN-PT can lead to a charge accumulation/depletion at the V_2O_3/PMN-PT interface. This can result in a modulation of V_2O_3 transport properties depending on the polarization direction in the PMN-PT. However, we observed that the zero-bias resistance of V_2O_3/PMN-PT devices is nearly identical when the substrate's polarization is switched toward (up) or away (down) from the V_2O_3 layer. This is inconsistent with the field-effect due to the polarization screening by free carriers in the V_2O_3. It is possible, however, that the absence of experimental evidence of the field-effect is due to a relatively large thickness of the V_2O_3 layer (close to 80-100 nm), because the field-effect is expected to be dominant only on the scale of Thomas-Fermi screening length, which typically does not exceed a few nanometers.

1. Dernier PD, Marezio M (1970) Crystal structure of the low-temperature antiferromagnetic phase of V_2O_3. *Phys Rev B* 2(9):3771.
2. McWhan DB, Menth A, Remeika JP, Brinkman WF, Rice TM (1973) Metal-insulator

transitions in pure and doped V_2O_3. *Phys Rev B* 7(5):1920.

3. Eckert LJ, Bradt RC (1973) Thermal expansion of corundum structure Ti_2O_3 and V_2O_3. *J Appl Phys* 44(8):3470.
4. Wongmaneerung R, Guo R, Bhalla A, Yimnirun R, Ananta S (2008) Thermal expansion properties of PMN-PT ceramics. *J Alloys Compd* 461(1–2):565.
5. Park SE, Shrout TR (1997) Ultrahigh strain and piezoelectric behavior in relaxor based ferroelectric single crystals. *J Appl Phys* 82(4):1804.
6. Austin IG (1962) The effect of pressure on the metal-to-Insulator transition in V_2O_3. *Philos Mag* 7(78):961.
7. Tagantsev AK, Cross LE, Fousek J (2010) *Domains in ferroic crystalls and thin films* (Springer).
8. Ramirez JG, et al. (2015) Effect of disorder on the metal-insulator transition of vanadium oxides: Local versus global effects. *Phys Rev B* 91(20):205123.
9. Del Valle J, et al. (2017) Electrically Induced Multiple Metal-Insulator Transitions in Oxide Nanodevices. *Phys Rev Appl* 8(5):054041.